# Lead-flux Growth of $Eu_4Ir_8As_7$ Crystals

Ulrike Pfannenschmidt and Rainer Pöttgen

Institut für Anorganische und Analytische Chemie, Universität Münster, Corrensstrasse 30, D-48149 Münster, Germany

Reprint requests to R. Pöttgen. E-mail: pottgen@uni-muenster.de

*Z. Naturforsch.* **2013**, *68b*, 1185 – 1190 / DOI: 10.5560/ZNB.2013-3228
Received August 26, 2013

Single crystals of the new arsenide $Eu_4Ir_8As_7$ were grown from a lead flux. The structure was refined on the basis of single-crystal X-ray diffractometer data: $Ca_4Ir_8P_7$ type, $P2_1/m$, $a = 1311.3(1)$, $b = 408.4(1)$, $c = 1360.3(1)$ pm, $\beta = 98.45(1)^\circ$, $wR2 = 0.0640$, 1985 $F^2$ values, 95 variables. The iridium and arsenic atoms in the $Eu_4Ir_8As_7$ structure build up a complex three-dimensional, covalently bonded $[Ir_8As_7]$ network with Ir–As distances ranging from 239 to 260 pm. Each iridium atom has three or four arsenic neighbors in slightly distorted trigonal-planar or tetrahedral coordination. The four crystallographically independent europium atoms fill cavities of coordination numbers 12, 13, and 15 (2 ×) within the $[Ir_8As_7]$ network. Parts of the $Eu_4Ir_8As_7$ structure resemble known simpler structure types, and one can describe the $Eu_4Ir_8As_7$ structure as an intergrowth variant of $CaBe_2Ge_2$-, TiNiSi- and $AlB_2$-related slabs.

*Key words:* Arsenide, Lead Flux, Crystal Structure

## Introduction

Ternary metal phosphides $A_xT_yP_z$ ($A$ = alkali, alkaline earth, electron-poor transition, or rare earth metals; $T$ = electron-rich transition metal) display a broad structural variety [1, 2]. Phosphides with a high metal content predominantly contain *isolated* phosphorus atoms, *i. e.* no P–P bonding occurs. With increasing phosphorus content one observes P–P bond formation. The most frequent (and smallest) substructure is the $P_2$ dumbbell, habitually observed with single bond character. Besides, many cage clusters, chains, and tubular substructures are known. The crystal chemical concepts of these materials are reviewed in [2].

The number of representatives decreases from the 3*d* to the 4*d* and 5*d* transition metals. This is not only a consequence of the price of the noble metals, but also due to the decreasing reactivity of especially the 5*d* elements. Classical solid-state synthesis of such phosphides requests repeated grinding, pelletizing and annealing of the samples in order to achieve product formation. A way out is the use of a low-melting metal flux [3 – 5] for the growth of small single crystals.

Due to the low reactivity, only few ternary iridium phosphides had been synthesized by heating mixtures of the elements in corundum crucibles [10, 11]. Most iridium phosphides were then synthesized with the help of lead or bismuth flux techniques. So far the following phosphides have structurally been characterized: $Mg_8Ir_{23}P_8$ [6], $Ca_2Ir_{12}P_7$ and $Ca_5Ir_{19}P_{12}$ [7], $AIrP$ ($A$ = Sr, Ba, La – Nd, Eu) [8, 9], $AIr_2P_2$ ($A$ = K, Rb, Cs, Ca, Sr, Ba, Eu) [8 – 12], $Ca_4Ir_8P_7$ [13], $Lu_3Ir_7P_5$ [14], $Sm_{15}Ir_{33}P_{26}$ [15], $Ce_4Ir_{13.55}P_9$ [16], $Ce_{13}Ir_{34.4}P_{24}$ [17], ScIrP [18], and the three series $RE_7Ir_{17}P_{12}$ ($RE$ = Y, Gd, Tb, Dy, Ho) [19], $RE_5Ir_{19}P_{12}$ [20] and $REIr_2P_2$ ($RE$ = La – Nd, Sm) [21, 22].

When it comes to the iridium arsenides, only the phases $REIr_2As_2$ ($RE$ = La – Nd [21], K, Rb [11], Cs [10], Sr [23]), $Mg_4Ir_7As_6$ [24], and $Ca_4Ir_8As_7$ [13] are known. In continuation of our work on rare earth metal-iridium-phosphides, we tested the lead-flux technique also for the arsenides. The crystal growth and structure refinement of the new arsenide $Eu_4Ir_8As_7$ are reported herein.

## Experimental

### *Synthesis*

Starting materials for the syntheses of $Eu_4Ir_8As_7$ were europium pieces (Johnson Matthey), iridium powder (Heraeus), arsenic pieces (Sigma-Aldrich), and lead granules (ABCR

GmbH), all with stated purities better than 99.9 %. The arsenic was purified by fractional sublimation under vacuum prior to use. First, the sesquioxide $As_2O_3$ was sublimed with the hot end of the sealed silica tube at 570 K and the other end at room temperature. After cutting off the cold end containing the sesquioxide the tube was sealed again, and the arsenic was sublimed with the hot end of the tube at 870 K. The lead granules were melted for 36 h at 770 K in an evacuated silica tube, followed by quenching and removing lead oxide from the surface (purification by liquation).

The elements were weighed in the ratio Eu : Ir : As : Pb = 4 : 8 : 7 : 60 and placed in a corundum crucible that was sealed in an evacuated quartz tube. The ampoule was heated in a muffle furnace at a rate of 20 K/h up to 1370 K and kept at that temperature for 100 h. Subsequently the sample was cooled to 970 K at a rate of 4 K/h and then to 570 K at 4 K/h. Finally the tube was cooled to room temperature by switching off the furnace. The excess lead flux was dissolved by a 1 : 1 molar mixture of $H_2O_2$ (ACROS 35 %) and glacial acetic acid (VWR International, > 99.8 %). The resulting sample was washed with demineralized water. The reaction product consisted of crystals of $IrAs_2$ [25], $EuIr_2As_2$ [26] and the new arsenide $Eu_4Ir_8As_7$. Similar by-products have also been observed during synthesis of $Ca_4Ir_8P_7$ and $Ca_4Ir_8As_7$ [13]. The $Eu_4Ir_8As_7$ crystals have metallic luster and are stable in moist air over months.

*EDX data*

The $Eu_4Ir_8As_7$ single crystals were analyzed by EDX with a Zeiss EVO® MA10 scanning electron microscope in variable pressure mode using $EuF_3$, Ir, and InAs as standards. Only europium, iridium and arsenic were observed by EDX. No contamination with the flux medium (lead) was evident.

*X-Ray diffraction*

Small pillar-shaped single crystals were glued to thin quartz fibres and investigated by Laue photographs in a Buerger camera (white molybdenum radiation; imaging plate technique, Fujifilm, BAS-1800). Intensity data of a suitable crystal were collected at room temperature by use of a Stoe IPDS-II image plate diffractometer using graphite-monochromatized Mo$K_\alpha$ radiation. A numerical absorption correction was applied to the data set. All relevant details concerning the data collection and evaluation are listed in Table 1.

*Structure refinement*

The data set showed a primitive monoclinic lattice. The systematic extinctions 0$k$0 only observed for $k = 2n$ led to the space groups $P2_1$ and $P2_1/m$ of which the centrosymmetric group was found to be correct during structure refinement.

Table 1. Crystal data and structure refinement for $Eu_4Ir_8As_7$.

| | |
|---|---|
| Empirical formula | $Eu_4Ir_8As_7$ |
| Formula weight, g mol$^{-1}$ | 2669.88 |
| Unit cell dimensions, pm | $a = 1311.3(1)$ |
| | $b = 408.4(1)$ |
| | $c = 1360.3(1)$ |
| Monoclinic angle, deg | $\beta = 98.45(1)$ |
| Cell volume, nm$^3$ | $V = 0.7206$ |
| Space group, $Z$ | $P2_1/m$, 2 |
| Pearson code | mP38 |
| Calculated density, g cm$^{-3}$ | 12.31 |
| Crystal size, $\mu$m$^3$ | $10 \times 10 \times 60$ |
| Transmission, max/min | 0.278/0.041 |
| Absorption coefficient, mm$^{-1}$ | 106.6 |
| $F$(000), e | 2198 |
| $\theta$ range for data collection, deg | 2 – 28 |
| Range in $hkl$ | ±17, ±5, ±17 |
| Total no. of reflections | 6609 |
| Independent reflections/$R_{int}$ | 1985/0.0558 |
| Reflections with $I > 2\,\sigma(I)/R_\sigma$ | 1679/0.0442 |
| Data/parameters | 1985/95 |
| Goodness-of-fit on $F^2$ | 1.066 |
| $R1/wR2$ for $I > 2\,\sigma(I)$ | 0.0298/0.0611 |
| $R1/wR2$ for all data | 0.0405/0.0640 |
| Extinction coefficient | 0.00074(5) |
| Largest diff. peak/hole, e Å$^{-3}$ | 2.98/–3.64 |

Table 2. Atomic coordinates and equivalent isotropic displacement parameters (pm$^2$) of $Eu_4Ir_8As_7$. All atoms lie on Wyckoff positions 2$e$ ($x$, 1/4, $z$). $U_{eq}$ is defined as one third of the trace of the orthogonalized $U_{ij}$ tensor.

| Atom | $x$ | $z$ | $U_{eq}$ |
|---|---|---|---|
| Eu1 | 0.78749(8) | 0.43644(7) | 50(2) |
| Eu2 | 0.48509(8) | 0.29128(7) | 47(2) |
| Eu3 | 0.71562(8) | 0.10300(7) | 66(2) |
| Eu4 | 0.89592(8) | 0.79382(8) | 78(2) |
| Ir1 | 0.65547(6) | 0.86139(5) | 37(2) |
| Ir2 | 0.27848(6) | 0.39834(5) | 35(2) |
| Ir3 | 0.08004(6) | 0.99817(5) | 49(2) |
| Ir4 | 0.57379(6) | 0.52968(5) | 34(2) |
| Ir5 | 0.94411(6) | 0.28020(5) | 37(2) |
| Ir6 | 0.44631(6) | 0.04838(5) | 41(2) |
| Ir7 | 0.33505(6) | 0.72813(6) | 57(2) |
| Ir8 | 0.01481(6) | 0.57311(5) | 38(2) |
| As1 | 0.25638(16) | 0.08147(14) | 45(4) |
| As2 | 0.09468(16) | 0.41280(14) | 45(4) |
| As3 | 0.46916(16) | 0.87272(14) | 42(4) |
| As4 | 0.15130(16) | 0.72081(14) | 42(4) |
| As5 | 0.39113(15) | 0.56188(14) | 38(4) |
| As6 | 0.68768(16) | 0.68933(14) | 39(4) |
| As7 | 0.94254(16) | 0.10087(15) | 53(4) |

The starting atomic parameters were derived from Direct Methods with SHELXS-97 [27, 28], and the structure was refined with anisotropic displacement parameters for the metal and isotropic ones for the arsenic atoms using SHELXL-97

Table 3. Interatomic distances (pm) for $Eu_4Ir_8As_7$. Standard deviations are equal or smaller than 0.2 pm. All distances of the first coordination spheres are listed.

| | | | | | | | | | | | |
|---|---|---|---|---|---|---|---|---|---|---|---|
| Eu1: | 2 | As5 | 311.0 | Ir2: | 2 | As6 | 243.8 | Ir8: | 1 | As4 | 248.7 |
| | 2 | As2 | 313.6 | | 1 | As2 | 244.7 | | 2 | As2 | 252.0 |
| | 2 | As4 | 314.6 | | 1 | As5 | 248.3 | | 1 | As2 | 255.4 |
| | 1 | Ir5 | 316.5 | | 2 | Ir4 | 288.5 | | 2 | Ir8 | 283.7 |
| | 1 | Ir4 | 324.1 | | 2 | Eu1 | 324.7 | | 2 | Ir5 | 285.1 |
| | 2 | Ir2 | 324.7 | | 1 | Eu2 | 325.9 | | 1 | Eu1 | 327.3 |
| | 2 | Ir7 | 327.2 | Ir3: | 1 | As1 | 242.1 | | 2 | Eu1 | 331.8 |
| | 1 | Ir8 | 327.3 | | 1 | As7 | 243.8 | As1: | 2 | Ir1 | 241.8 |
| | 2 | Ir8 | 331.8 | | 2 | As7 | 244.0 | | 1 | Ir3 | 242.1 |
| Eu2: | 2 | As6 | 309.0 | | 2 | Ir3 | 293.4 | | 1 | Ir6 | 259.5 |
| | 2 | As5 | 313.7 | | 1 | Eu4 | 340.4 | | 2 | Eu3 | 329.7 |
| | 2 | As3 | 314.6 | | 2 | Eu4 | 346.6 | | 2 | Eu4 | 346.9 |
| | 2 | Ir7 | 316.0 | Ir4: | 1 | As6 | 244.8 | As2: | 1 | Ir2 | 244.7 |
| | 1 | Ir2 | 325.9 | | 2 | As5 | 247.0 | | 1 | Ir5 | 247.1 |
| | 1 | Ir6 | 326.8 | | 1 | As5 | 249.8 | | 2 | Ir8 | 252.0 |
| | 2 | Ir1 | 328.0 | | 2 | Ir4 | 284.7 | | 1 | Ir8 | 255.4 |
| | 1 | Ir4 | 328.0 | | 2 | Ir2 | 288.5 | | 2 | Eu1 | 313.6 |
| | 2 | Ir4 | 335.4 | | 1 | Eu1 | 324.1 | | 2 | Eu4 | 349.1 |
| Eu3: | 1 | Au7 | 298.0 | | 1 | Eu2 | 328.0 | As3: | 1 | Ir7 | 243.8 |
| | 2 | Ir7 | 321.5 | | 2 | Eu2 | 335.4 | | 1 | Ir6 | 245.2 |
| | 2 | As3 | 322.3 | Ir5: | 2 | As4 | 239.4 | | 1 | Ir1 | 247.0 |
| | 1 | Ir1 | 326.5 | | 1 | As7 | 243.7 | | 2 | Ir6 | 249.0 |
| | 2 | As1 | 329.7 | | 1 | As2 | 247.1 | | 2 | Eu2 | 314.6 |
| | 2 | Ir6 | 341.1 | | 2 | Ir8 | 285.1 | | 2 | Eu3 | 322.3 |
| | 2 | As4 | 342.5 | | 1 | Eu1 | 316.5 | As4: | 2 | Ir5 | 239.4 |
| Eu4: | 1 | As6 | 288.7 | | 2 | Eu4 | 319.4 | | 1 | Ir7 | 239.7 |
| | 2 | As7 | 313.3 | Ir6: | 1 | As3 | 245.2 | | 1 | Ir8 | 248.7 |
| | 2 | Ir5 | 319.4 | | 2 | As3 | 249.0 | | 2 | Eu1 | 314.6 |
| | 1 | Ir3 | 340.4 | | 1 | As1 | 259.5 | | 2 | Eu3 | 342.5 |
| | 1 | Ir1 | 341.2 | | 2 | Ir1 | 281.8 | As5: | 2 | Ir4 | 247.0 |
| | 2 | Ir3 | 346.6 | | 2 | Ir6 | 290.3 | | 1 | Ir7 | 247.9 |
| | 2 | As1 | 346.9 | | 1 | Eu2 | 326.8 | | 1 | Ir2 | 248.3 |
| | 2 | As2 | 349.1 | | 2 | Eu3 | 341.1 | | 1 | Ir4 | 249.8 |
| Ir1: | 2 | As1 | 241.8 | Ir7: | 1 | As4 | 239.7 | | 2 | Eu1 | 311.0 |
| | 1 | As6 | 243.9 | | 1 | As3 | 243.8 | | 2 | Eu2 | 313.7 |
| | 1 | As3 | 247.0 | | 1 | As5 | 247.9 | As6: | 2 | Ir2 | 243.8 |
| | 2 | Ir6 | 281.8 | | 2 | Eu2 | 316.0 | | 1 | Ir1 | 243.9 |
| | 1 | Eu3 | 326.5 | | 2 | Eu3 | 321.5 | | 1 | Ir4 | 244.8 |
| | 2 | Eu2 | 327.9 | | 2 | Eu1 | 327.2 | | 1 | Eu4 | 288.7 |
| | 1 | Eu4 | 341.2 | | | | | | 2 | Eu2 | 309.0 |
| | | | | | | | | As7: | 1 | Ir5 | 243.7 |
| | | | | | | | | | 1 | Ir3 | 243.8 |
| | | | | | | | | | 2 | Ir3 | 244.0 |
| | | | | | | | | | 1 | Eu3 | 298.0 |
| | | | | | | | | | 2 | Eu4 | 313.3 |

(full-matrix least-squares on $F_o^2$) [29, 30]. The structure refinement revealed the composition $Eu_4Ir_8As_7$. A look into the Pearson data base [31] readily showed isotypism with $Ca_4Ir_8P_7$ and $Ca_4Ir_8As_7$ [13]. The setting of the calcium compounds was used in the subsequent cycles. To check for deviations from the ideal composition, the occupancy parameters were refined in separate series of least-squares cycles. All sites were fully occupied within three standard deviations. The final difference Fourier synthesis revealed no residual peaks. The refined atomic positions, displacement parameters, and interatomic distances are given in Tables 2 and 3.

Further details of the crystal structure investigation may be obtained from Fachinformationszentrum Karlsruhe, 76344 Eggenstein-Leopoldshafen, Germany (fax: +49-7247-808-666; e-mail: crysdata@fiz-karlsruhe.de, http://www.fiz-karlsruhe.de/request_for_deposited_data.html) on quoting the deposition number CSD-426592.

## Discussion

So far $Eu_4Ir_8As_7$ and $EuIr_2As_2$ [26] are known in the ternary system Eu-Ir-As. $EuIr_2As_2$ crystallizes with a pronounced $CaBe_2Ge_2$ subcell (space group $P4/nmm$) and shows modulation along the crystallographic $c$ direction. The shortest interatomic distances in the $Eu_4Ir_8As_7$ structure occur between the iridium and arsenic atoms with Ir–As distances ranging

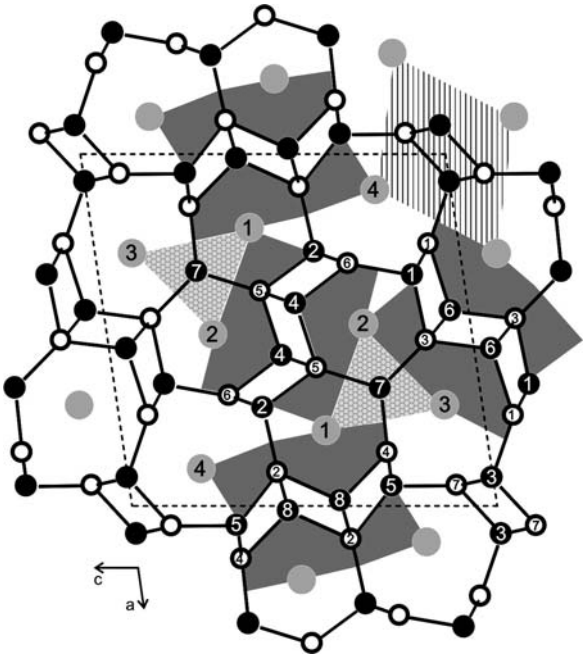


Fig. 1. Projection of the $Eu_4Ir_8As_7$ structure along the short unit cell axis. Europium, iridium and arsenic atoms are drawn as medium grey, black filled and open circles, respectively. The three-dimensional polyanionic $[Ir_8As_7]$ network and atom designations are given. The $ThCr_2Si_2$- (gray shading), TiNiSi- (dashed shading) and $AlB_2$- (honeycomb shading) related slabs are emphasized at the right-hand part of the drawing.

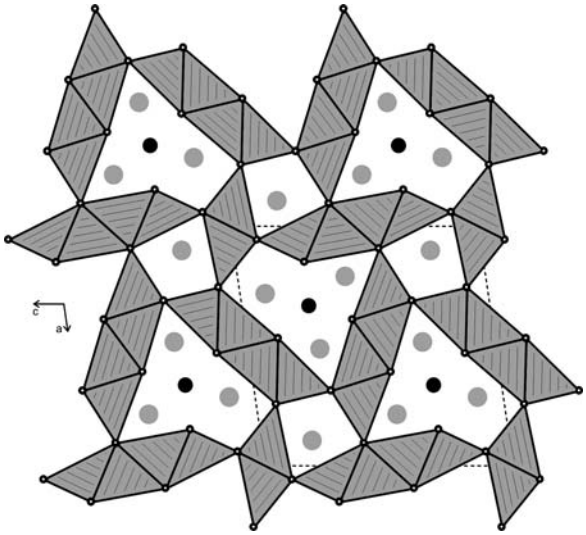

Fig. 2. View of the $Eu_4Ir_8As_7$ structure along the short unit cell axis. Europium, iridium and arsenic atoms are drawn as medium grey, black filled and open circles, respectively. The network of condensed $IrAs_4$ tetrahedra of the Ir1, Ir2, Ir3, Ir4, Ir5, Ir6, and Ir8 atoms is emphasized. The Ir7 atoms have trigonal-planar arsenic coordination.

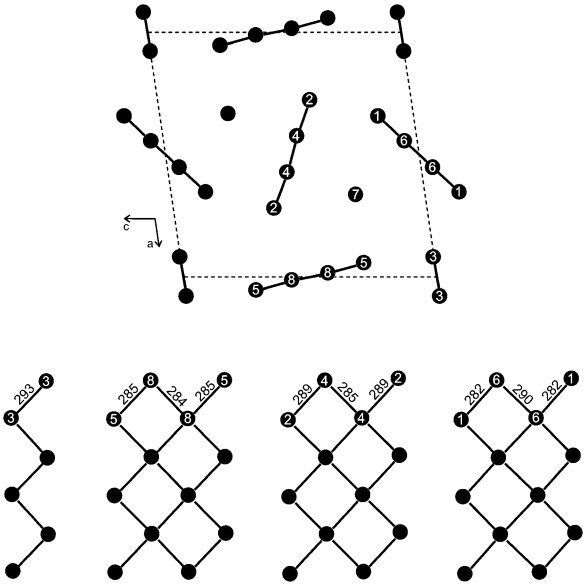


Fig. 3. Top: Projection of the iridium substructure of $Eu_4Ir_8As_7$ onto the *ac* plane. Bottom: Cutout of the four substructures perpendicular to the projection direction. Atom designations and interatomic distances are given. Ir7 has no iridium neighbors.

from 239 to 260 pm, close to the sum of the covalent radii [32] of 247 pm. Together, the iridium and arsenic atoms build up a complex three-dimensional, covalently bonded $[Ir_8As_7]$ network which leaves larger cages for the europium atoms.

A projection of the $Eu_4Ir_8As_7$ structure along the monoclinic axis is presented in Fig. 1. The eight crystallographically independent iridium atoms belong to different substructures as emphasized by different shadings. The Ir7 atoms have trigonal-prismatic europium coordination, similar to many $AlB_2$-related ternary phases (honeycomb-shading). The Ir3 atoms (dashed shading) have distorted tetrahedral arsenic coordination. This substructure corresponds to the family of TiNiSi compounds [33]. The largest substructure comprises the atoms Ir1, Ir2, Ir4, Ir5, Ir6, and Ir8 (grey shading). This part of the structure has a $CaBe_2Ge_2$-related arrangement, as has recently been observed for the arsenides $REIr_2As_2$ ($RE$ = La – Nd) [21]. Consequently one can describe the $Eu_4Ir_8As_7$ structure as an intergrowth variant of $AlB_2$-, TiNiSi- and $CaBe_2Ge_2$-related slabs. Similar slabs also occur in the metal-rich ternary iridium phosphides [14 – 20].

The tetrahedral coordination of Ir1, Ir2, Ir3, Ir4, Ir5, Ir6, and Ir8 is emphasized in Fig. 2. These $IrAs_4$ tetra-

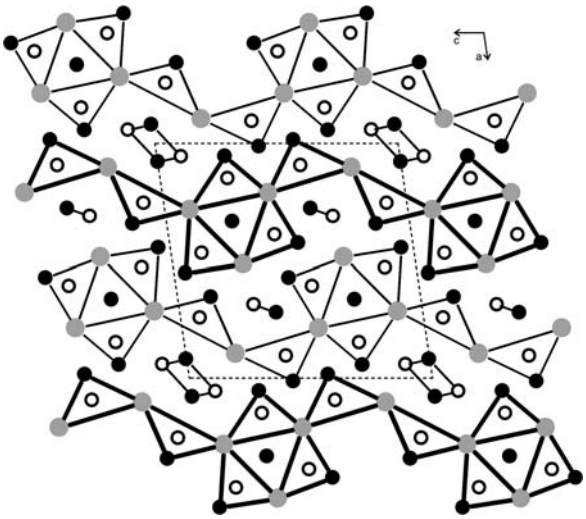

Fig. 4. Projection of the $Eu_4Ir_8As_7$ structure along the short unit cell axis. Europium, iridium and arsenic atoms are drawn as medium grey, black filled and open circles, respectively. The arsenic-filled trigonal prisms are emphasized. The condensed units drawn by thin and thick lines are shifted with respect to each other by half a translation period.

hedra share common corners and edges, leading to a three-dimensional network. The larger cavities left by this network of tetrahedra are filled by the Ir7-centered trigonal europium prisms (formed by Eu1, Eu2, and Eu3) and the Eu4 atoms.

Within the $[Ir_8As_7]$ network we observe a quite narrow range of Ir–Ir distances from 282 to 293 pm, only slightly longer than in *fcc* iridium with 272 pm Ir–Ir [34]. The iridium substructure is shown in Fig. 3. The Ir7 atoms within the $AlB_2$ slab have no direct iridium neighbors. The shortest Ir7–Ir7 distance of 408 pm corresponds to the *b* lattice parameter. The Ir3 atoms form zig-zag chains that extend in the *b* direction. The larger grids of the Ir5–Ir8, Ir2–Ir4, and Ir1–Ir6 substructures also extend along *b* and can be considered as two condensed zig-zag chains. Very similar iridium substructures with comparable ranges of Ir–Ir distances have been observed in the many $RE_xIr_yP_z$ phases [7, 13 – 20]. Thus, besides Ir–As bonding, the $Eu_4Ir_8As_7$ structure is also stabilized by weak Ir–Ir bonding.

The four crystallographically independent europium atoms have coordination numbers (CN) ranging from 12 to 15 with iridium and arsenic atoms in their coordination shells. There are no direct Eu–Eu interactions. The shortest Eu–Eu distances of 408 pm correspond to the *b* lattice parameter. Although all europium atoms are part of the $CaBe_2Ge_2$-related slabs, they have a reduced coordination number as compared to $CeIr_2As_2$ with CN 16 (8 As + 8 Ir) [21]. This is a consequence of the intergrowth character, since all europium atoms are located at the sectional areas between the slabs.

Finally we draw back to the coordination of the arsenic atoms. Most of them are located in distorted trigonal prisms formed by the europium and iridium atoms (Fig. 4). These prisms share the triangular faces along the *b* axis and common edges in *ac* direction, leading to strands that run along *c*. Adjacent strands are shifted by half the *b* translation period with respect to each other. This presentation is solely based on the geometrical motif; however, such propeller-like substructures can easily be distinguished from each other. This building pattern is similar to the structural chemistry of metal-rich phosphides [1, 2].

*Acknowledgement*

This work was supported by the Deutsche Forschungsgemeinschaft through SPP 1458 *Hochtemperatursupraleitung in Eisenpnictiden*.

[1] Yu. Kuz'ma, S. Chykhrij in *Handbook on the Physics and Chemistry of Rare Earths*, (Eds.: K. A. Gschneidner, Jr., L. Eyring), Vol. 23, Elsevier Science, Amsterdam, **1996**, Chapter 156, pp. 285 – 433.
[2] R. Pöttgen, W. Hönle, H. G. von Schnering in *Encyclopedia of Inorganic Chemistry*, 2nd ed., (Ed.: R. B. King), Vol. VII, Wiley, New York, **2005**, pp. 4255 – 4308.
[3] P. C. Canfield, Z. Fisk, *Phil. Mag. B* **1992**, *6*, 1117.
[4] M. G. Kanatzidis, R. Pöttgen, W. Jeitschko, *Angew. Chem. Int. Ed.* **2005**, *44*, 6996.
[5] P. C. Canfield, *Phil. Mag. B* **2012**, *92*, 2398.
[6] A. Löhken, A. Imre, A. Mewis, *Z. Anorg. Allg. Chem.* **2007**, *633*, 137.
[7] A. Wurth, A. Löhken, A. Mewis, *Z. Anorg. Allg. Chem.* **2002**, *628*, 661.
[8] C. Lux, A. Mewis, S. Junk, A. Gruetz, G. Michels, *J. Alloys Compd.* **1993**, *200*, 135.
[9] A. Löhken, G. J. Reiß, D. Johrendt, A. Mewis, *Z. Anorg. Allg. Chem.* **2005**, *631*, 1144.
[10] A. Czybulka, M. Noack, H.-U. Schuster, *Z. Anorg. Allg. Chem.* **1992**, *609*, 122.
[11] P. Wenz, H.-U. Schuster, *Z. Naturforsch.* **1984**, *39b*, 1816.
[12] A. Löhken, C. Lux, D. Johrendt, A. Mewis, *Z. Anorg. Allg. Chem.* **2002**, *628*, 1472.
[13] A. Löhken, A. Mewis, *Z. Anorg. Allg. Chem.* **2004**, *630*, 2418.
[14] U. Pfannenschmidt, U. Ch. Rodewald, R. Pöttgen, *Z. Anorg. Allg. Chem.* **2010**, *636*, 314.
[15] U. Pfannenschmidt, U. Ch. Rodewald, R. Pöttgen, *Z. Kristallogr.* **2010**, *225*, 280.
[16] U. Pfannenschmidt, U. Ch. Rodewald, R. Pöttgen, *Z. Naturforsch.* **2011**, *66b*, 7.
[17] U. Pfannenschmidt, U. Ch. Rodewald, R. Pöttgen, *Z. Kristallogr.* **2011**, *226*, 229.
[18] U. Pfannenschmidt, U. Ch. Rodewald, R. Pöttgen, *Z. Naturforsch.* **2011**, *66b*, 205.
[19] U. Pfannenschmidt, R. Pöttgen, *Intermetallics* **2011**, *19*, 1052.
[20] U. Pfannenschmidt, U. Ch. Rodewald, R.-D. Hoffmann, R. Pöttgen, *J. Solid State Chem.* **2011**, *184*, 2731.
[21] U. Pfannenschmidt, F. Behrends, H. Lincke, M. Eul, K. Schäfer, H. Eckert, R. Pöttgen, *Dalton Trans.* **2012**, *41*, 14188.
[22] V. A. Ivanshin, E. M. Gataullin, A. A. Sukhanov, U. Pfannenschmidt, R. Pöttgen, *J. Phys.: Conf. Ser.* **2012**, *391*, 012024.

[23] A. Imre, A. Hellmann, G. Wenski, J. Graf, D. Johrendt, A. Mewis, *Z. Anorg. Allg. Chem.* **2007**, *633*, 2037.
[24] A. Wurth, A. Löhken, A. Mewis, *Z. Anorg. Allg. Chem.* **2001**, *627*, 1213.
[25] A. Kjekshus, *Acta Chem. Scand.* **1971**, *25*, 411.
[26] U. Pfannenschmidt, Dissertation, Westfälische Wilhelms-Universität Münster, Münster, **2011**.
[27] G. M. Sheldrick, SHELXS-97, Program for the Solution of Crystal Structures, University of Göttingen, Göttingen (Germany) **1997**.
[28] G. M. Sheldrick, *Acta Crystallogr.* **1990**, *A46*, 467.
[29] G. M. Sheldrick, SHELXL-97, Program for the Refinement of Crystal Structures, University of Göttingen, Göttingen (Germany) **1997**.
[30] G. M. Sheldrick, *Acta Crystallogr.* **2008**, *A64*, 112.
[31] P. Villars, K. Cenzual, *Pearson's Crystal Data – Crystal Structure Database for Inorganic Compounds* (release 2012/13), ASM International, Materials Park, Ohio (USA) **2012**.
[32] J. Emsley, *The Elements*, Oxford University Press, Oxford **1999**.
[33] R.-D. Hoffmann, R. Pöttgen, *Z. Kristallogr.* **2001**, *216*, 127.
[34] J. Donohue, *The Structures of the Elements*, Wiley, New York **1974**.